



Roll waves on a shallow layer of a dilatant fluid

Sandro Longo*

Department of Civil Engineering, University of Parma, Viale G.P. Usberti, 181/A, 43100 Parma, Italy

ARTICLE INFO

Article history:

Received 6 January 2010
 Received in revised form
 2 September 2010
 Accepted 9 September 2010
 Available online 17 September 2010

Keywords:

Roll waves
 Free surface instabilities
 Granular flows
 Dilatant fluids

ABSTRACT

This paper is about the free surface instabilities of granular flows, usually called roll waves. A shallow layer of shear-thickening fluid ($\tau = a(\partial u/\partial y)^n$ with $n = 2$) is considered to study finite-amplitude permanent roll waves down a slope, simplified by Karman's momentum integral approach. The existence of conditions of a periodic discontinuous solution is derived, as smooth profiles with depth increasing monotonically between periodic shocks. Energy dissipation in the body of the stream and in the discontinuity is analysed and discussed. Two conditions are derived. The first is related to the physically acceptable shape of the smooth profiles, and the second is related to positive energy loss across the shock. These conditions can be converted into a limiting discharge, viewed in the fixed frame, and in a limiting flow thickness (or limiting Froude number), for the permanent periodic roll wave to exist without further conditions. A minimum-length roll wave (MLRW) is defined as the periodic permanent roll waves with zero energy dissipation in the shock. The MLRW also requires a limiting value of the Froude number to exist.

© 2010 Elsevier Masson SAS. All rights reserved.

1. Introduction

Free surface instabilities of flows down inclined channels have been widely observed in Newtonian and non-Newtonian fluids. Natural gravity flows as debris flows are recorded in many areas and are a constant reminder of the need for prediction and control. In most cases, these flows manifest a succession of waves which, given enough space, develop into long waves. This behaviour is common to water and many non-Newtonian fluids. The observations of roll waves in the torrents in the late 19th century were followed by the description reported in Cornish [1]. Several authors in many areas have reported observations of roll waves in mud flows. The widespread formation of free surface instabilities, independent of the rheological properties of the fluid, is due to the effects of inertia: if the flow field could adjust its characteristics instantaneously, it would respond to a variation of the current depth reducing the local mean velocity, and the wave would simply be a kinematic wave. In real situations, the response is delayed, and an increased current depth enhances a positive mass flux, leading to the growth of the perturbation [2]. In addition, the presumed structure of the wall boundary layer favours the growth of the perturbations: the adverse gradient pressure acts to destabilize the boundary layer, reducing the wall friction and accelerating the wave crest [3]. Dressler [4] also emphasised the need for a friction reduction in the flow direction, from smaller to larger water depths, in order to obtain roll waves. Although the

rheological properties of the fluid do not control the instability mechanism, all the characteristics of the development of the wave depend on those properties.

The first study of the phenomenon was based on linear-stability analysis of the basic equations written in the long-wave approximation and applied to the laminar current. It is possible to predict the threshold and growth of the waves. In most cases, laminar Newtonian flows are analysed, deriving the Orr–Sommerfeld equation for the amplitude of the perturbation [5–7]. A similar result was obtained by Chen [8], using the shallow-water equation but including the spatial variation of the momentum coefficient.

In turbulent flow in rectangular channels, assuming a Chézy resistance law with a constant coefficient, Jeffreys [9], Stoker [10] and Liggett [11] found a critical Froude number of 2. Several researchers, among them Iwasa [12], Koloseus and Davidian [13], and Berlamont and Vanderstappen [14] highlighted the strong sensitivity of the critical Froude number on the velocity profile, the Reynolds number, and friction law. In particular, according to Rouse [15] and Rosso et al. [16], the Darcy–Weisbach friction factor increases along with the Froude number in supercritical streams. According to Brock [17–19], no firm conclusion on such a dependence can be drawn, because experimental data are not accurate enough, especially the measurements of water depth. Moreover, an apparent increment in the friction factor could better be explained as an energy transfer from mean flow to waves (the limiting case is a stationary wave, with finite amount of energy and zero net flux).

Dressler [4] developed the finite-amplitude wave theory. In his paper, Dressler described that the discontinuous periodic solutions

* Tel.: +39 0521905157; fax: +39 0521905924.
 E-mail address: sandro.longo@unipr.it.

Nomenclature

a	Dimensional parameter in the friction law
b	Non-dimensional parameter
b_{crit}, b'_{crit}	First, second critical value of the non-dimensional parameter b
c, c_{crit}	Celerity of the wave, critical value of the celerity of the wave c
F, F_{crit}, F'_{crit}	Froude number, first/second critical Froude number
f_{crit}	Function in critical condition
g	Acceleration due to gravity
H	Height of the shock
J	Energy slope
K	Constant discharge per unit width in the moving frame
l	Length scale
m	Resistance coefficient in the Chezy formula for Newtonian fluids
n	Fluid index
q	Discharge per unit width
r	Ratio of the normal stress in the x and in the y direction
t	Time
u, U	Depth average velocity
U_b, U_f	Depth average velocity in the back/front section
U_c	Depth average velocity in the critical section
U_n	Normal velocity
v_x	Main stream fluid velocity component
x, ξ	Longitudinal coordinate
y, Y	Depth of the flow
Y_b, Y_f	Depth of the flow in the back/front section
Y_c	Flow depth in the critical section
Y_{lim}	Limiting flow depth for instability growth
Y_{max}	Maximum flow depth
Y_n	Normal depth of the flow
Y_1^*, Y_2^*	Real positive solution of the numerator of the wave profile
$\alpha, \alpha_b, \alpha_f$	Energy flux factor, in the back/front section
β, β_b, β_f	Momentum flux factor, in the back/front section
$\gamma = \rho g$	Specific weight
ΔP	Rate of change of mechanical energy in the shock
ΔE_j	Energy dissipated in the shock
ΔE_f	Mean energy dissipated for friction in a wavelength
λ, λ_{min}	Length of the wave, minimum value
ρ	Mass density
τ_b	Average boundary shear stress
θ	Bottom inclination
*	Operator indicating the non-dimensional value

are obtained by joining Bresse profiles with shocks. Dressler's theory, originally developed for fully turbulent flows, was extended to laminar flows for Newtonian fluids by Ishihara et al. [20] and to power-law fluids by Ng and Mei [21], who essentially focussed on pseudoplastic fluids (mud) and detailed the analysis only for shear thinning fluids. Prasad et al. [22] applied Dressler's theory to flowing dry grains at moderate low void concentration (the interparticle fluid is air). In their analysis, which was based on experiments, the writers assume that a large increase in the volumetric solid fraction takes place near the front of the wave. They approximate the depth-averaged dispersed flow of the grain in a manner similar to those of shallow fluid flow.

In addition, several laboratory experiments with water streams were conducted by Ishihara et al. [20], Mayer [23], Brock [18], and Julien and Hartley [24,25].

Most of the results available refer to the limit condition for the existence of roll waves, but no one can infer the determination of all roll-wave parameters (wavelength, wave height, celerity) for a given system. There are some experimental indications from Ponce and Maisner [26], who, using Brock's data [18], found that the observed periodic roll waves match the maximum growth rate (in linear-stability analysis). Referring to frequency, Kapitza [27] suggested that all waves are expected to be unstable, and the least unstable are selected by the system. He also suggested that the observed waves have the maximum absolute rate of energy dissipation. A different criterion is developed by Ng and Mei [21], who infer that the observed roll wave has the lowest amplitude corresponding to no energy loss across the shock.

Kranenburg [28] has shown that short wavelength roll waves are unstable to subharmonic disturbances, the growth of which annihilates the roll waves through the mechanism of shock coalescence and develop into roll waves of larger size. It holds true, as output of numerical integration, for small-amplitude waves, and brings to a long roll wave even though no limits to the length is given nor experimental verification is available.

We need to mention that the existence of natural roll waves (i.e. not forced at the inlet, but developed as a natural growing of instabilities) requires a minimum length of a given channel, as pointed out by Montuori [29] for turbulent conditions and by Julien and Hartley [25] for laminar conditions. Such minimum length can be extreme, making difficult the experimental observation of natural roll waves, in particular at low Froude number. Considering that the nature of roll waves in a dilatant fluid is the same than for Newtonian fluids, we can infer that a minimum length is also required for granular flows in dense regimes.

In this paper, Dressler's theory is extended to granular flows in dense regimes. The friction law for dry, granular materials flowing in a dense regime is a subject for research; our assumptions are a simplification. In the present analysis, it is assumed that grains behave like a power-law fluid, with a fluid index (the exponent of the shear rate in the constitutive equation) of $n = 2$. Dilatant fluids in which $n = 2$ were experimentally described and modelled by Bagnold [30] for granular mixture at a relatively high shear rate. They also correspond to dry, granular material at large grain-volume concentrations and moderate shear rates. We will assume this value for the fluid index, because it allows some analytical solutions which are representative of numerical solutions obtainable for a different value, but we need to mention that Chen and Ling [31,32] and Hunt et al. [33] revisited Bagnold's data and concluded that the value of the fluid index is ~ 1.5 . It is assumed that the fluid is homogeneous and that no segregation occurs.

Roll waves have been observed in experimental debris flows in a rigid bed flume with heterogeneous sediment and almost constant volume concentration [34], developing with characteristics similar to water flow roll waves. Usually most debris flows take the form of strongly transient flows, often as almost periodic surges separated by relatively low flow rate. To explain such behaviour hydraulic instability is often cited in the literature.

The necessity to include the free surface waves in modelling natural debris flows is required by a proper dimensioning of some countermeasures to reduce the risk and the damage associated with debris flows. Amongst debris flow countermeasures, direction controlling works are used to guide to safe place the stream. These works are excavated channels with cross section large enough to handle peak flow discharge levels, i.e. the surges occurring in roll waves [35].

The roll waves herein described are periodic, discontinuous solutions with a discontinuity (shock) connecting a smooth profile in a shallow-flow approximation. The waves are permanent and move downstream with a celerity higher than the maximum fluid

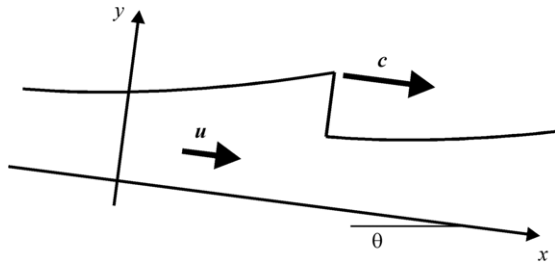


Fig. 1. Schematic of periodic waves with sharp front in shallow fluid flows.

velocity. We do not analyse stability of such special roll waves and we assume that energy balance can control periodic permanent roll waves. This is a pragmatic approach, even though we are aware that a combination of criteria based on energy considerations and stability could be a more complete approach to the problem.

The next section is devoted to deriving the basic equations applying Karman’s momentum integral method and in Section 3 the description of the ‘special solution’ is reported, obtaining a first admissibility condition detailed in Section 4. Some wave characteristics are briefly described in Section 5. Shock conditions and energy dissipation in the shock are analysed in Sections 6 and 7. The limiting discharge and the energy balance analysis in the unstable stream are analysed in Sections 8 and 9. Discussions and conclusions are given in Sections 10 and 11. The detailed computations are reported in Appendices A–C.

2. Balance and conservation equations

Let us consider a 2D flow of a fluid down a plane of inclination θ . The coordinate system has the x -axis along the bed and the y -axis normal to it (Fig. 1). For long waves, we can assume that variations in the flow occur on lengths larger than the thickness. Applying Karman’s momentum integral method to mass conservation and linear momentum balance, we obtain the following set of equations for a wide channel:

$$\begin{cases} y_{,t} + (uy)_{,x} = 0 & (a) \\ u_{,t} + \beta uu_{,x} - (\beta - 1) \frac{u}{y} y_{,t} + rg \cos \theta y_{,x} + u^2 \beta_{,x} & (1) \\ = g \sin \theta - \frac{\tau_b}{\rho y} & (b) \end{cases}$$

where u is the depth average velocity of flow function of the longitudinal coordinate x at time t , y is the depth of the flow, β is the momentum flux factor (equal to 5/4 for a dilatant fluid in laminar condition and with $n = 2$, [2, Eq. (2.16)]), and r is the ratio of the normal stress in the x -direction to the normal stress in the y -direction. τ_b is the boundary shear stress and ρ is the mass density. The first equation is the mass conservation; the second equation is the momentum balance equation. For non-uniform flow, r could depend on the divergence of the flow [36] but many numerical simulations have shown that this ratio is equal to ~ 1 for dense granular flows. For instance, Ertas et al. [37] found $0.97 < r < 1.02$.

Introducing a moving reference having celerity c , and assuming that in the moving reference the chosen state variables U and Y are functions of $\xi = x - ct$ only (Fig. 2):

$$\begin{aligned} u(x, t) &= U(x - ct) = U(\xi) \\ y(x, t) &= Y(x - ct) = Y(\xi). \end{aligned} \quad (2)$$

The two equations (1)(a) and (1)(b) become

$$\begin{cases} (UY)_{,\xi} - cY_{,\xi} = 0 & (a) \\ -cU_{,\xi} + \beta UU_{,\xi} + c(\beta - 1) \frac{U}{Y} Y_{,\xi} + rg \cos \theta Y_{,\xi} & (3) \\ = g \sin \theta - \frac{\tau_b}{\rho Y} & (b) \end{cases}$$

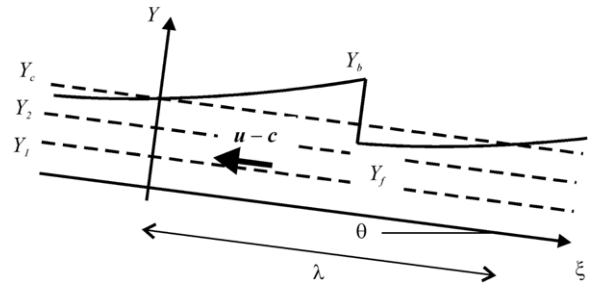


Fig. 2. Definition sketch of a roll-wave profile in the moving frame.

where the spatial variation of the momentum flux correction term has been dropped, even though this term should always be retained in order to satisfy the principle of frame indifference [8].

Eqs. (3)(a) and (3)(b) can be rearranged as

$$\begin{cases} U_{,\xi} = \frac{g \left(\sin \theta - \frac{\tau_b}{\rho Y} \right) (U - c)}{[(U - c)(\beta U - c) - c(\beta - 1)U - rgY \cos \theta]} & (a) \\ Y_{,\xi} = - \frac{gY \left(\sin \theta - \frac{\tau_b}{\rho Y} \right)}{[(U - c)(\beta U - c) - c(\beta - 1)U - rgY \cos \theta]} & (b) \end{cases} \quad (4)$$

$\gamma = \rho g$ is the specific weight. Dividing the two equations and integrating results:

$$U = \frac{(cY - K)}{Y}. \quad (5)$$

K is the constant discharge per unit width in the moving frame. It was denoted as ‘overrun’ by Chow [38] and ‘progressive discharge’ by Dressler [4]. The discharge in the fixed frame varies with space and time.

For a dilatant power-law fluid with $n = 2$, the bottom shear stress in a wide channel is

$$\tau_b = \rho a \frac{U^2}{Y^2} \quad (6)$$

and the energy slope is $j = aU^2/gY^3$, where a is a parameter (depending on the density, size, concentration of grains, and internal friction for a granular mixture) with the dimension of a square length.

On using (4)(b) and (5), the profile equation for progressing waves reads:

$$Y_{,\xi} = \frac{[gY^5 \sin \theta - a(cY - K)^2]}{Y^2 (c^2 \beta Y^2 - c^2 Y^2 + rgY^3 \cos \theta - \beta K^2)}. \quad (7)$$

Assuming a length scale for both horizontal and vertical directions $l = c^2/g$, Eq. (7) can be written in non-dimensional form as

$$Y_{,\xi^*}^* = \sin \theta \frac{[Y^{*5} - b(Y^* - K^*)^2]}{Y^{*2} (\beta Y^{*2} - Y^{*2} + rY^{*3} \cos \theta - \beta K^{*2})} \quad (8)$$

where $b = \frac{a}{\sin \theta} \frac{g^2}{c^4}$, $Y_{(\cdot)}^* = Y_{(\cdot)} g/c^2$, $\xi^* = \xi g/c^2$, $K^* = Kg/c^3$ (c is the velocity scale, $l = c^2/g$ is the length scale for both horizontal and vertical directions, $g =$ acceleration due to gravity).

3. The ‘special solution’

Owing to the kinds of functions obtained by integrating Eq. (8) (logarithm, hyperbolic function, polynomials), no periodic solution is forecast for the wave profile. A possible solution is a discontinuous periodic solution, piecing together continuous profiles with shocks. Such a solution was suggested by Dressler [4] for Newtonian fluid. Dressler named it the ‘special solution’, and we will follow the same definition. As for a Newtonian fluid, the solution has to admit a region with supercritical mean velocity and a second

region with sub-critical mean velocity (in the moving reference). The two regions are separated by a critical section with mean velocity equal to the critical velocity. The flow depth in the critical section is Y_c^* .

There is experimental evidence that a roll-wave profile in a Newtonian fluid has a finite steepness in the critical section. We assume that this holds true also for roll waves in a granular flow. In Appendix A, we demonstrate that no solution with an inflection point is possible.

As a consequence, the possible periodic solution requires that the critical depth also be a root of the numerator in Eq. (8) in order to have a finite steepness. The pole in $Y^* = Y_c^*$ must be erased. The result is that both numerator and denominator vanish in Y_c^* :

$$\begin{cases} Y_c^{*2}(\beta - 1) + rY_c^{*3} \cos \theta - \beta(1 - U_c^*)^2 Y_c^{*2} = 0 & \text{(a)} \\ Y_c^{*2} - bU_c^{*2} = 0 & \text{(b)} \end{cases} \quad (9)$$

Solving Eq. (9)(a), we obtain the mean velocity in the critical section:

$$U_{c1,2}^* = 1 \mp \sqrt{1 - \frac{1}{\beta} + \frac{r \cos \theta}{\beta} Y_c^*} \quad (10)$$

where only the solution with the negative sign satisfies the condition of roll waves' existence $U^* < 1$ ($c > U$, [39]).

On using Eqs. (10) and (9)(b) yields

$$Y_c^{*3} - \frac{br \cos \theta}{\beta} Y_c^* - 2b + \frac{b}{\beta} + 2b \sqrt{1 - \frac{1}{\beta} + \frac{r \cos \theta}{\beta} Y_c^*} = 0. \quad (11)$$

The interesting positive real solution can be obtained numerically for fixed values of the parameters. The critical stream depth is weakly influenced by bottom slope (it increases for increasing bottom slope); it also increases for decreasing value of the ratio r (not shown).

The apparent discharge is also constrained. Using mass conservation and Eq. (9)(a) results in

$$K^{*2} = \frac{Y_c^{*2}(\beta - 1) + rY_c^{*3} \cos \theta}{\beta}. \quad (12)$$

Substituting Eq. (12) in the wave profile (Eq. (8)) (and considering that both numerator and denominator vanish in the critical section), results in

$$Y_{,\xi^*}^* = \sin \theta \frac{\left[Y_c^{*4} + Y_c^{*3} Y_c^{*3} + Y_c^{*2} Y_c^{*2} + (Y_c^{*3} - b) Y_c^* + \frac{bY_c^*}{\beta} [(\beta - 1) + Y_c^* r \cos \theta] \right]}{Y_c^{*2} [(\beta - 1)(Y_c^* + Y_c^*) + r \cos \theta (Y_c^{*2} + Y_c^* Y_c^* + Y_c^{*2})]}. \quad (13)$$

4. Limiting condition for a positive steepness of the profile

In order to construct roll waves from the previous profile, it is necessary that $\frac{dY^*}{d\xi^*} \Big|_{Y_c^*} > 0$. The denominator in (13) is always positive. In the critical section, we simply have to make the numerator positive also

$$4Y_c^{*3} + \frac{br}{\beta} Y_c^* \cos \theta - \frac{b}{\beta} > 0 \quad (14)$$

by assuming that $Y_c^* > 0$.

Using Vandermonde determinants, we can conclude that of the three roots of the polynomial inequality (14), one is real (Y_{c1}^*) and the two others are complex conjugate (Y_{c2}^* and Y_{c3}^*), because the inequality

$$\frac{1}{4} \left(\frac{b}{\beta} \right)^2 + \frac{1}{27} \left(\frac{br}{\beta} \cos \theta \right)^3 > 0 \quad (15)$$

is always satisfied. The real root can be obtained in explicit form and is always positive. Inequality (14) is satisfied if $Y_c^* > Y_{c1}^*$.

Having stated that, of the three solutions, two are complex conjugates, without losing the information on the behaviour of the real (and positive) solution, we can substitute the cubic term in Eq. (11) into Eq. (14). Inequality (15) is now written as

$$\frac{5r \cos \theta}{\beta} Y_c^* + 8 - \frac{5}{\beta} > 8 \sqrt{\left(1 - \frac{1}{\beta} + \frac{r \cos \theta}{\beta} Y_c^* \right)}. \quad (16)$$

The argument of the square root is always positive. Squaring the left and right sides results in

$$Y_c^{*2} (25r^2 \cos^2 \theta) + Y_c^* (16\beta r \cos \theta - 50r \cos \theta) + 25 - 16\beta > 0. \quad (17)$$

Inequality (17) is satisfied if $Y_c^* > \frac{1}{r \cos \theta}$ and $Y_c^* < \frac{25-16\beta}{25r \cos \theta}$. Let us verify inequality (17) for the two limits. Substituting the first limit in (18) results in

$$\frac{4}{r^3 \cos^3 \theta} > 0 \quad (18)$$

which is always satisfied. Substituting the second limit results in

$$-\frac{16b}{25} + 4 \left(\frac{25 - 16\beta}{25r \cos \theta} \right)^3 > 0 \quad (19)$$

which is satisfied if

$$b < b_{\text{crit}} = \frac{25}{4} \left(\frac{25 - 16\beta}{25r \cos \theta} \right)^3. \quad (20)$$

The inequality (20) can also be expressed as

$$c > c_{\text{crit}} = \left(\frac{ag^2 r^3}{\tan \theta (1 + \tan^2 \theta)} \frac{4}{25} \left(\frac{25}{25 - 16\beta} \right)^3 \right)^{1/4}. \quad (21)$$

In this form, our findings indicate that, for a given bottom inclination and a given rheological parameter of the dilatant fluid, only waves with celerity higher than the critical celerity can propagate. Considering that roll waves can exist only if the condition $c > U$ [39] is satisfied, if $U > c_{\text{crit}}$, the Whitham inequality $c > U$ is dominant and also automatically satisfies the condition $c > c_{\text{rit}}$. If $U < c_{\text{crit}}$, Eq. (21) can be extended in the form $c > c_{\text{crit}} > U$ and permanent periodic finite-amplitude roll waves can exist only if they have a celerity greater than the critical celerity. Using the resistance law, the discharge per unit width q has a limit given by the following inequality:

$$\left(\frac{gq^3 \sin \theta}{a} \right)^{1/5} < \left(\frac{ag^2 r^3}{\tan \theta (1 + \tan^2 \theta)} \frac{4}{25} \left(\frac{25}{25 - 16\beta} \right)^3 \right)^{1/4}. \quad (22)$$

Eq. (22) can be solved in terms of the stream depth for the stable flow with the following result:

$$Y^* < Y_{\text{crit}}^* \equiv \left(\frac{4}{25} \right)^{1/6} \sqrt{br \cos \theta \left(\frac{25}{25 - 16\beta} \right)}. \quad (23)$$

Later, we shall verify that a second limit on the existence of roll waves is related to the energy balance in the shock. Both limits shall be discussed in Section 10.

For comparison, in a Newtonian fluid and for $\beta = 1$, assuming a Chézy formula $j = \frac{m^2 u^2}{g y}$, the necessary condition for roll waves derived imposing the positive steepness is $4m^2 < \tan \theta$ [4]; making $c > U$, Dressler's condition is equivalent to $c > c_{\text{crit}} = 2\sqrt{gY \cos \theta}$.

5. Wave characteristics

It can be demonstrated that the numerator of the wave profile between two subsequent shocks (Eq. (13)) has two real, positive solutions and two complex, conjugate solutions. The profile can be integrated obtaining a function $\xi^*(Y^*)$ involving logarithms and trigonometric functions (see Appendix B). The length of the wave is equal to

$$\lambda^* = \xi^*(Y_b^*) - \xi^*(Y_f^*). \tag{24}$$

The average depth of the roll-wave profile is

$$\langle Y^* \rangle = \frac{1}{\lambda^*} \int_{Y_f^*}^{Y_b^*} Y^* \frac{d\xi^*}{dY^*} dY^* \tag{25}$$

and the average discharge rate is

$$\langle q^* \rangle \equiv U_n^* Y_n^* = \frac{1}{\lambda^*} \int_0^{\lambda^*} U^* Y^* d\xi^* \tag{26}$$

where U_n^* and Y_n^* are the normal velocity and flow depth. Using Eq. (5) in non-dimensional form and spatially averaging results in

$$\langle Y^* \rangle - \langle q^* \rangle = K^*. \tag{27}$$

6. Shock conditions

The shock condition is obtained from the mass conservation and momentum balance equations for a control volume across the shock:

$$\begin{cases} c [Y]_f^b = [UY]_f^b & (a) \\ c [UY]_f^b = \left[\beta U^2 Y + \frac{1}{2} g Y^2 r \cos \theta \right]_f^b & (b) \end{cases} \tag{28}$$

where the square brackets are the operator $[\langle \cdot \rangle]_f^b = \langle \cdot \rangle|_b - \langle \cdot \rangle|_f$ and b and f stand for the two control sections, back and front. The weight of the roller and bottom friction have been neglected. In extended and non-dimensional form, the mass conservation equation (28)(a) is

$$(1 - U_b^*) Y_b^* = (1 - U_f^*) Y_f^* = K^*. \tag{29}$$

The linear momentum balance equation (28)(b) can be written as

$$\begin{aligned} 2(Y_b^* - Y_f^*) - 2(\beta_b Y_b^* - \beta_f Y_f^*) + 2K^{*2} \left(\frac{\beta_f Y_b^* - \beta_b Y_f^*}{Y_b^* Y_f^*} \right) \\ + 4K^* (\beta_b - \beta_f) = (Y_b^* - Y_f^*) (Y_f^* + Y_b^*) r \cos \theta \end{aligned} \tag{30}$$

where Eq. (12) has already been used.

For $\beta_b = \beta_f = \beta$, it reduces to

$$\begin{aligned} 2(1 - \beta)(Y_b^* - Y_f^*) + 2\beta K^{*2} \left(\frac{Y_b^* - Y_f^*}{Y_b^* Y_f^*} \right) \\ = (Y_b^* - Y_f^*) (Y_f^* + Y_b^*) r \cos \theta. \end{aligned} \tag{31}$$

The condition $Y_f^* = Y_b^*$ is not compatible with the assumption $\beta_b \neq \beta_f$, because (31) reduces to

$$-\frac{2}{Y} (\beta_b - \beta_f) (Y^* - K^*)^2 = 0 \tag{32}$$

which is satisfied only for $\beta_b = \beta_f$. Neglecting the trivial solution $Y_f^* = Y_b^*$ (no shock), (31) can be solved, obtaining the following relation:

$$Y_b^* = - \left(\frac{Y_f^*}{2} + \frac{\beta - 1}{r \cos \theta} \right) + \sqrt{\left(\frac{Y_f^*}{2} + \frac{\beta - 1}{r \cos \theta} \right)^2 + \frac{2\beta K^{*2}}{Y_f^* r \cos \theta}} \tag{33}$$

where $Y_b^* > Y_f^* > 0$. On using mass conservation (12), it reads as

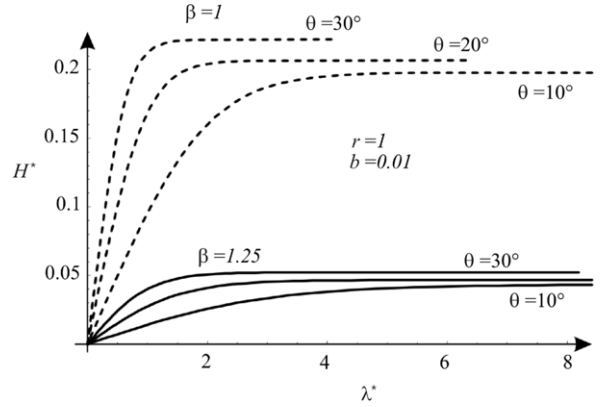


Fig. 3. Height of the shock vs. wavelength. The curves correspond to the condition $r = 1$ and $b = 0.01$.

$$\begin{aligned} Y_b^* = - \left(\frac{Y_f^*}{2} + \frac{\beta - 1}{r \cos \theta} \right) \\ + \sqrt{\left(\frac{Y_f^*}{2} + \frac{\beta - 1}{r \cos \theta} \right)^2 + \frac{2Y_c^{*2} (\beta - 1 + Y_c^* r \cos \theta)}{Y_f^* r \cos \theta}}. \end{aligned} \tag{34}$$

The zero wavelength $\lambda^* \rightarrow 0$ corresponds to $Y^* \rightarrow Y_c^*$. The maximum wavelength $\lambda^* \rightarrow \infty$ corresponds to the maximum depth in front of the shock (and the maximum wave height), and is obtained for $Y_f^* \rightarrow Y_2^*$:

$$\begin{aligned} Y_{\max}^* = - \left(\frac{Y_2^*}{2} + \frac{\beta - 1}{r \cos \theta} \right) \\ + \sqrt{\left(\frac{Y_2^*}{2} + \frac{\beta - 1}{r \cos \theta} \right)^2 + \frac{2Y_c^{*2} (\beta - 1 + Y_c^* r \cos \theta)}{Y_2^* r \cos \theta}}. \end{aligned} \tag{35}$$

It decreases for larger values of β and for larger values of r (not shown). The height of the shock is given by $H^* = Y_b^* - Y_f^*$ and is reported vs. the wavelength in Fig. 3, for various slopes and flux conditions. It tends to asymptotic values slightly dependent on bottom inclination and is strongly influenced by the value of β .

7. Energy dissipation in the shock

The rate of change of mechanical energy across the jump is equal to the following [39]:

$$\begin{aligned} \Delta P = \left[\int_0^Y \left(\left(\frac{1}{2} \rho v_x^2 + \rho g y \cos \theta \right) (v_x - c) \right. \right. \\ \left. \left. + \rho g r \cos \theta (Y - y) v_x \right) dy \right]_{Y_f}^{Y_b}. \end{aligned} \tag{36}$$

Here, v_x is the main stream fluid velocity component; the first term in the argument of the integral represents the energy variation, including the bodily transport across the boundary, and the second term is the rate of working by the normal stress at the boundary. The effects of bottom friction and body forces have been neglected. Eq. (36) can be expressed in function of the depth average velocity as

$$\begin{aligned} \Delta P^* = -\frac{1}{2} \left(1 - \frac{K^*}{Y_b^*} \right)^2 Y_b^* \left(\alpha_b - \alpha_b \frac{K^*}{Y_b^*} - \beta_b \right) \\ + \frac{1}{2} \left(1 - \frac{K^*}{Y_f^*} \right)^2 Y_f^* \left(\alpha_f - \alpha_f \frac{K^*}{Y_f^*} - \beta_f \right) \end{aligned}$$

$$\begin{aligned}
 & -\cos\theta \left[\frac{Y_b^{*2}}{2} \left(r - \frac{K^*}{Y_b^*} (1+r) \right) \right. \\
 & \left. - \frac{Y_f^{*2}}{2} \left(r - \frac{K^*}{Y_f^*} (1+r) \right) \right] \quad (37)
 \end{aligned}$$

where α is the energy flux factor. For a dilatant fluid with $n = 2$ and in laminar motion, $\alpha = 75/44 \simeq 1.705$ [21].

Substituting the expression for discharge in the moving frame and dividing by the discharge per unit width in the moving frame, the energy drop across the jump, assuming $\alpha_b = \alpha_f = \alpha$ and $\beta_b = \beta_f = \beta$, is

$$\begin{aligned}
 \Delta E_j^* = & \frac{(Y_b^* - Y_f^*)}{4Y_b^* Y_f^*} \left\{ -\sqrt{\frac{2Y_b^* Y_f^*}{\beta(\beta - 1 + r \cos\theta(Y_b^* + Y_f^*))}} \right. \\
 & \times \left[(3\alpha - \alpha\beta - \beta - \beta^2) + 3(\beta - \alpha)r \cos\theta(Y_b^* + Y_f^*) \right] \\
 & + \frac{1}{\beta} \left[\alpha(1 - \beta)(Y_b^* + Y_f^*) - \alpha r \cos\theta(Y_b^* + Y_f^*)^2 \right. \\
 & \left. \left. + 4\beta r \cos\theta Y_b^* Y_f^* \right] \right\}. \quad (38)
 \end{aligned}$$

For $\alpha = \beta = 1$ and for $r = 1$, (38) has the classical expression:

$$\Delta E_j^* = -\cos\theta \frac{(Y_b^* - Y_f^*)^3}{4Y_b^* Y_f^*}. \quad (39)$$

Having neglected the thermal energy contribution, a necessary condition for a physically based shock is $\Delta E_j^* < 0$, that is, the shock dissipates mechanical energy. The (mechanical) energy dissipation condition in the shock limits the admissible values of Y_f^* and Y_b^* . Some results are shown in Fig. 4. The physically admissible area is the region $Y_f^* < Y_b^*$, also contoured by a curve $f_{crit}(Y_f^*, Y_b^*) = 0$ in which $\Delta E_j^* > 0$. Note that if $\alpha = \beta = 1$ and $r = 1$, the critical curve has equation $Y_f^* = Y_b^*$, and the finite-amplitude shocks always dissipate energy, whereas for different values of the flux factors and of the parameter r , finite-amplitude shock without energy dissipation is possible.

A sensitivity analysis indicates that increasing the bottom inclination moves the critical curve towards higher values of front/back stream depth. A reduction of the ratio r enlarges the closed-hatched area, corresponding to energy production in the jump (physically impossible). A reduction in the two factors α and β moves the critical curve towards modest values of the front/back stream depth.

If different factors are assumed, namely increasing the value of factors from the minimum depth to the maximum depth, a double band of wavelength with finite-amplitude shocks without energy loss is allowed (not shown).

The limitation due to energy dissipation condition in the shock corresponds to a limitation in wave height ($Y_f^* - Y_b^*$) and is equivalent to imposing a minimum wavelength. (Wavelength increases with the wave height.)

A second limitation on the maximum value of the parameter b is obtained by observing the energy balance in the hydraulic jump and the function $Y_b^*(Y_f^*)$, describing the possible back–front heights compatible with the mass and momentum balance for a control volume across the shock. The curves are reported for different values of the parameter b in Fig. 5.

In this figure a critical value b'_{crit} of b is reported, which is explained in the following.

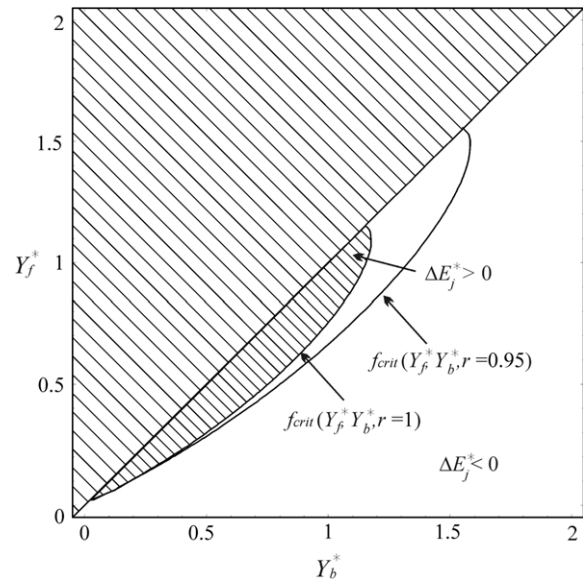


Fig. 4. Energy balance in the jump. The hatched area is unacceptable, because $Y_f^* > Y_b^*$. The close-hatched area corresponds to energy production in the jump, physically impossible. $\beta = 1.25$, $\alpha = 1.705$, $\theta = 30^\circ$. The two f_{crit} curves correspond to $r = 1$ and $r = 0.95$.

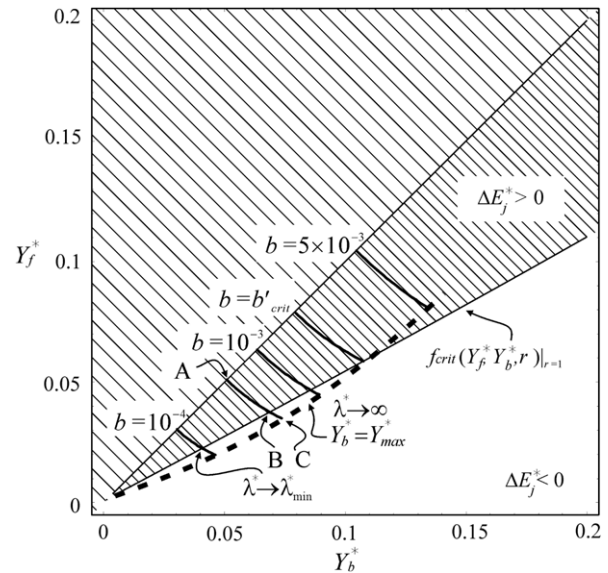


Fig. 5. Energy and momentum balance in the jump. The hatched area is unacceptable, because $Y_f^* > Y_b^*$. The closed-hatched area corresponds to energy production in the jump, physically impossible. The thick curves satisfy the momentum balance across the shock, for different values of the parameter b . The dashed-thick curve represents the maximum layer thickness, in front of the shock, for different values of the parameter b , and corresponds to an infinite wavelength. The limiting value b'_{crit} corresponds with a maximum height coincident with zero energy dissipation in the jump (and also $\lambda_{min}^* = \lambda_{\infty}^*$). $\beta = 1.25$, $\alpha = 1.705$, $\theta = 30^\circ$, $r = 1$, $b'_{crit} = 0.00216$.

Let us consider the thick curve corresponding to $b = 5 \times 10^{-4}$. The starting point A is on the line $Y_b^* = Y_f^*$ but it is not admissible because it is in the region of energy production in the shock, which is unphysical. The first useful point is B, at the intersection with the curve $f_{crit}(Y_f^*, Y_b^*, r = 1) = 0$, where the wavelength has the minimum possible value λ_{min}^* and the shock is energetically admissible. Moving from point B to point C the wavelength increases and reaches an infinite value at point C, where the maximum flow depth is reached. For $b = b'_{crit}$ the two points B and C collapse. In this condition a maximum flow depth

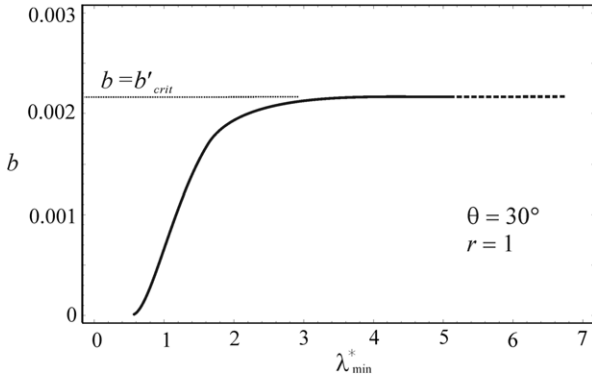


Fig. 6. Minimum wavelength compatible with energy dissipation in the shock. The dashed branch is not admissible because it does not satisfy the criterion of energy dissipation in the shock. $\beta = 1.25$, $\alpha = 1.705$, $\theta = 30^\circ$, $b'_{crit} = 0.00216$.

Y_b^* also satisfies the zero energy dissipation in the jump in a roll wave having infinite wavelength. The critical value b'_{crit} is obtained by numerically solving a strongly nonlinear system of equations representing energy dissipation and momentum balance in the shock.

The minimum wavelength vs. the parameter b is shown in Fig. 6, for flow conditions identical to those which refer to the diagram in Fig. 5. The critical value of the parameter b fixed by the existence condition of the wave profile (see Appendix A) is generally larger than b'_{crit} . For instance, for the flow conditions of the test reported in Figs. 5 and 6 we have $b_{crit} \equiv 0.07698 > b'_{crit}$.

The condition $b < b'_{crit}$ is equivalent to

$$c > c'_{crit} = \left(\frac{ag^2}{b'_{crit} \sin \theta} \right)^{1/4} \quad (40)$$

and with the same reasoning reported in Section 4 requires that

$$Y^* < Y'_{crit} \equiv \left(\frac{b^3}{b'_{crit}} \right)^{1/6} \quad (41)$$

Similar results were obtained by Ng and Mei [21] for mud flows. On using the dissipation energy criterion in the shock, they obtained a minimum discharge in the moving frame (equivalent to a maximum discharge in the fixed frame), a minimum celerity of the roll waves and a maximum wave number (corresponding to a minimum wavelength). As for the limit described in Section 4, this is not a necessary condition for roll waves, because the condition $c > U > c'_{crit}$ also satisfies the Whitham criterion [39]. In Section 10, there is a discussion of limiting discharge as computed using limits (23) and (41).

7.1. The minimum-length roll wave (MLRW)

The requirement of a minimum energy dissipation in the shock is met by the waves with a wavelength equal to λ_{min}^* . Herein, these waves are called MLRW. The computation of the relevant characteristics of the MLRW is carried out as follows:

- (i) for given $b (< b'_{crit})$, θ , α , β , r , evaluate λ_{min}^* , Y_b^* and Y_f^* ;
- (ii) evaluate Y_c^* and K^* by solving (11) and (12);
- (iii) solve for the average depth and the average discharge in the fixed frame
- (iv) on using the velocity law

$$\frac{U}{\sqrt{gY}} = Y \sqrt{\frac{\sin \theta}{a}} \quad (42)$$

as obtained using (6), evaluate the normal velocity and the Froude number as

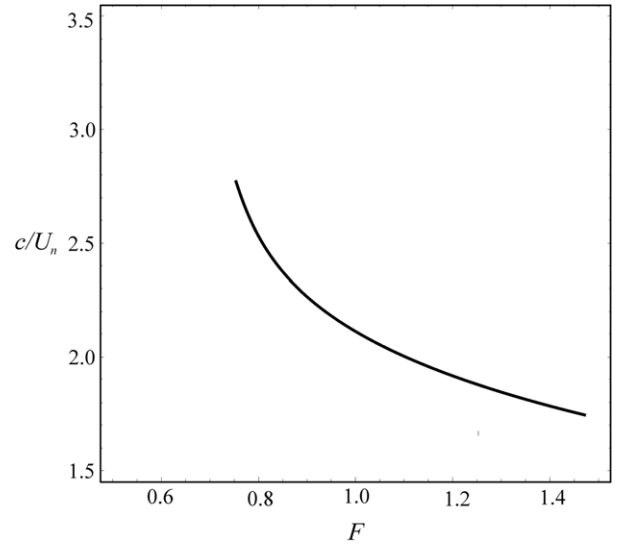


Fig. 7. Phase celerity as a function of the Froude number, $\beta = 1.25$, $\alpha = 1.705$, $r = 1$.

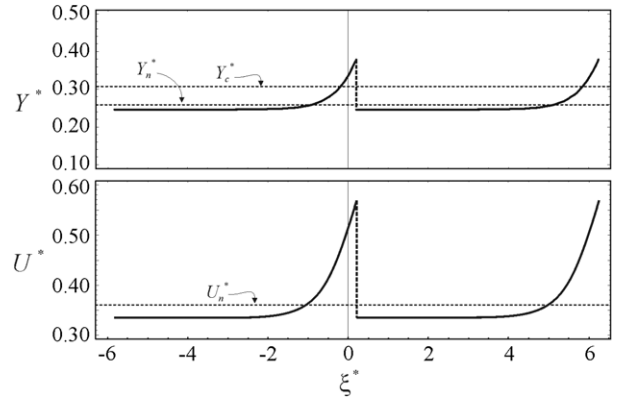


Fig. 8. Profiles computed for a MLRW. $\beta = 1.25$, $\alpha = 1.705$, $r = 1$, $b = 0.00216$, $\theta = 30^\circ$.

$$Y_n^* = b^{1/5} (q^*)^{2/5} \quad (43)$$

$$F = \frac{Y_n^*}{\sqrt{b \cos \theta}} \quad (44)$$

The non-dimensional wave celerity is obtained as

$$\frac{c}{U_n} = \sqrt{\frac{b}{Y_n^{*3}}} \quad (45)$$

In Fig. 7, the MLRW celerity as obtained in the present model is reported as a function of the Froude number, while in Fig. 8 the wave profile, wave velocity and bottom stress are reported for a MLRW.

8. Limiting discharge

In the present model, two possible limiting mechanisms are detected. The first is related to the physical evidence of a positive steepness of the roll waves in the critical section [4, see Appendix A]. The second is related to the energy balance in the shock. Both mechanisms limit the value of the parameter b ; these limits can be converted into a limiting thickness of the (normal) flow (Eqs. (23) and (34)), even though they do not represent a necessary condition for the existence of roll waves. They can be better converted in terms of a limiting Froude number.

If we express the Froude number corresponding to the limit in (23) (first critical Froude number), we obtain

$$F_{\text{crit}} = \frac{U_{\text{crit}}}{\sqrt{gY_{\text{crit}} \cos \theta}} \equiv Y_{\text{crit}} \sqrt{\frac{\tan \theta}{a}} \equiv \frac{1}{(b_{\text{crit}})^{1/6} \sqrt{\cos \theta}} \quad (46)$$

$$\equiv \frac{1}{\left(\frac{25}{4}\right)^{1/6} \sqrt{\frac{25-16\beta}{25r}}}$$

The first critical Froude number $F_{\text{crit}} = F_{\text{crit}}(\beta, r)$ is independent of the bottom inclination and the rheological parameters of the granular medium. For $\beta = 1.02$ (turbulent flow) and $r = 1$, we have $F_{\text{crit}} = 1.25$, while for $\beta = 1.25$ (laminar flow) and $r = 1$, $F_{\text{crit}} = 1.65$.

If we express the Froude number corresponding to the limit in (34) (the second critical Froude number), we obtain

$$F'_{\text{crit}} = \frac{U'_{\text{crit}}}{\sqrt{gY'_{\text{crit}} \cos \theta}} \equiv Y'_{\text{crit}} \sqrt{\frac{\tan \theta}{a}} \equiv \frac{1}{(b'_{\text{crit}})^{1/6} \sqrt{\cos \theta}} \quad (47)$$

The computed value of F'_{crit} does not depend on the value of the parameter a ; using the computed values of b'_{crit} , its results do not depend on bottom inclination and are constant for given values of α , β and r , i.e., $F'_{\text{crit}} = F'_{\text{crit}}(\alpha, \beta, r)$ with $b'_{\text{crit}} \propto \cos^{-3} \theta$. For $\alpha = 1.03$, $\beta = 1.02$ (turbulent flow) and $r = 1$, we have $F'_{\text{crit}} = 1.496 \pm 0.001$; for $\alpha = 1.704$, $\beta = 1.25$ (laminar flow) and $r = 1$, $F'_{\text{crit}} = 2.99 \pm 0.01$, while for $r = 0.9$ in laminar flow, $F'_{\text{crit}} = 3.04 \pm 0.01$.

According to the present model finite-amplitude periodic roll waves are unconditionally allowed above the limit corresponding to F'_{crit} , while they are allowed only if they satisfy the condition $c > c_{\text{crit}}$ below F_{crit} .

9. Energy dissipation in the unstable stream

The mean energy dissipated for friction in a wavelength is computed in non-dimensional form as

$$\Delta E_f^* = -b \sin \theta \int_{Y_f^*}^{Y_b^*} \frac{U^{*2}}{Y^{*3}} \frac{1}{Y_{,\xi}^*} dY^* \quad (48)$$

which can be written as

$$\Delta E_f^* = -b \sin \theta \int_{Y_f^*}^{Y_b^*} \frac{\left(1 - \frac{Y_c^*}{Y^*} \sqrt{\frac{\beta - 1 + rY_c^* \cos \theta}{\beta}}\right)^2}{Y^{*3}} \frac{1}{Y_{,\xi}^*} dY^* \quad (49)$$

A stream in steady, uniform motion obviously results in $\Delta E_f^* + \lambda^* \sin \theta = 0$ for any value of the wavelength λ^* . In the presence of roll waves, including the energy dissipated in the jump, the energy balance over a wavelength results in

$$\Delta E^* = \Delta E_f^* + \Delta E_j^* + \lambda^* \sin \theta. \quad (50)$$

Assuming a friction law in non-uniform, unsteady motion equal to the friction law in steady, uniform motion, the energy budget is generally a negative function. That is, the system dissipates more energy than the energy gained from gravity.

The results of numerical integration are shown in Fig. 9. In the vertical, the percentage of extra energy dissipation with respect to the stable uniform stream is reported. The starting point corresponds to the MLRW, and all the curves have a maximum value decreasing for lower bottom inclination. The jump enhances dissipation, and the stream in unstable motion dissipates more than the equivalent stream in stable, steady, uniform motion (*equivalent* means having the same average discharge with identical channel characteristics). All the computations have neglected the finite size of the moving shock, the contribution of the weight of the grains in the shock, and the curvature of the trajectories. It has been demonstrated that for roll waves in water streams, inclusion of the weight

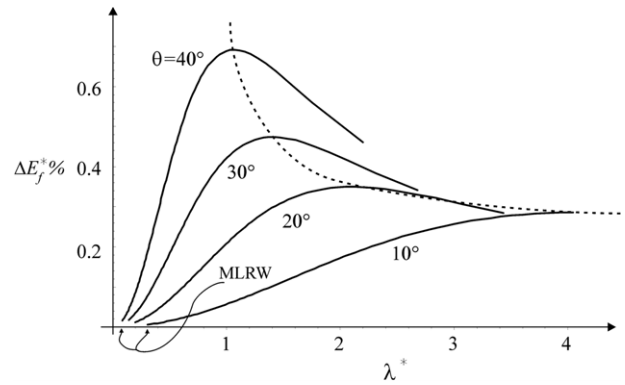


Fig. 9. Extra dissipation due to friction. $\beta = 1.25$, $b = 0.01$, $r = 1$.

of the fluid in the jump in linear momentum balance across the shock tends to reduce the ratio Y_b^*/Y_f^* [19] and favours smaller wavelengths. Surface tension contrasts the growth of instabilities and rounds the wave crest [40] and the energy balance is very sensitive to small variations in the parameters. Also, the assumption of a different friction law gives different results. In a dry, granular stream, surface tension is not present, but all the other mentioned factors are present. According to Kapitza [27] and Ng and Mei [21], the observed roll wave has the smallest mean energy averaged over the wavelength. Such a roll wave clearly meets the condition of finite-amplitude shock with zero dissipation across it and has back/front depth on the critical curve, but still dissipates more energy than the energy gained. Dressler's hypothesis (that a roll wave with a minimum of dissipated energy could be present and hence could be the stable solution) unfortunately, is not borne out, at least for granular flows. Unless a different friction law is included, to manage the boundary layer structure in the presence of adverse gradient pressure, the energy budget is negative. Also, computing the energy budget of the MLRW for varying b (and hence for varying wave celerity c at a given bottom inclination θ) results in a monotonic function, with extra dissipation increasing with decreasing b . This result is not of much help in determining the stable permanent roll wave.

10. Discussion

The present model, developed for finite-amplitude permanent periodic waves, suggests a stabilizing effect of an increased discharge, even though experiments are necessary to better quantify the effects and to extend the validity of the approach to other granular media. Some doubts about the stability of the permanent periodic roll waves still remain. We need to mention that reports on experiments on roll waves in water [18] make a substantial difference between natural and periodic roll waves. The former spontaneously appear in a channel as a result of amplification of natural (non-imposed) disturbances and are generally not periodic; the latter are periodic and are usually obtained by forcing the inlet with a paddle and by adjusting the amplitude and period of the paddle motion. This means that roll waves (in water) are not necessarily periodic, and if periodic roll waves are stable, they need a minimum length of the channel to become permanent. This minimum length of the channel is of the order of thousands wavelengths and imposes severe restrictions on its feasibility in the laboratory. If the results for roll waves in water hold true also for granular roll waves, a typical length scale for the channel should be of the order of several tens of meters. We can infer that roll waves in a much shorter channel are presumably not 'mature', in the sense that they have not acquired stable characteristics (if any). It is also difficult to verify that they are strictly periodic.

On the basis of the results obtained, two main indications arise. The first is that the resistance law adopted cannot be fully correct in the unsteady motion analysed and the boundary layer structure should be included in order to explain a reduced friction and dissipation; the second is that we can infer that permanent roll waves, as described in the present analysis, cannot completely fill the flow system. They have to coexist with other waves which dissipate less than the energy gained from gravity, leaving the excess for satisfying the energy balance. Otherwise, all the experimentally observed roll waves are unstable [27], and would disappear if enough space were given (not necessarily recovering a uniform stream).

Experimental investigations of roll waves in granular flows may be of considerable help to further analysis. The new experiments should be designed also with the aim of increasing the height of the roll wave and the general vertical scale of the flow, in order to eliminate some concerns that naturally arise modelling with a continuum model a phenomenon where the flow depth can be of the order of a few grain diameters.

It can be debated if the finite-amplitude permanent periodic waves herein described are real and can have physical sense. There are two important different approaches to the roll wave problem: the first is based on stability, the second is based on energy considerations.

The Kranenburg [28] results would suggest that instability of short wavelength to longer wavelength perturbations ultimately lead to wave mergers and the coarsening of wave trains. As a consequence, nonlinear interaction dynamics would control completely roll waves, whereas the shock properties would play no role.

Dressler [4], Ng and Mei [21], Prasad et al. [22] based their analysis on the role played by energy in selecting finite-amplitude roll waves and deal with permanent periodic waves. In the case of a Newtonian fluid the properties of the minimum permanent periodic roll wave (shortest wavelength and lowest amplitude without energy loss in the shock) appear to be consistent with the experimental data [21]. Also Prasad et al. [22], who carried out a parametric study on a Dressler like model applied to a shallow layer of flowing grains, obtained results well correlated with their experimental data.

We share the opinion that a combination of criteria based on energy consideration and linearised instability can be a reasonable approach for studying roll waves [21]. It is plausible that the initial waves that appear are related to the most unstable linear waves, and the final waves are those that are selected by nonlinear interactions, but a class of free surface instabilities belongs to permanent periodic waves as those analysed in the present study.

11. Conclusions

The proposed solution for finite-amplitude roll waves in a dilatant fluid shares many similarities with the solution proposed by Dressler [4] for a Newtonian fluid and by Ng and Mei [21] for mud. The solution is expressed as a discontinuous function obtained by connecting two continuous profiles with a shock. The continuous profiles are obtained in the shallow equation approximation.

- In order to construct the profile between two shocks, it is necessary that the steepness of the wave be finite and positive in the section where critical condition is reached. It results in the inequality $b < b_{crit}$, b being a non-dimensional group based on rheological characteristics of the fluid, wave celerity, and bottom inclination. The inequality can be converted into a limiting minimum wave celerity for given rheological parameters and bottom inclination and in a limiting (mean) flow rate in the fixed frame. It can also be converted into a limiting stream depth or a limit Froude number, which fixes

a threshold to the permanent periodic wave existence without further conditions. This critical threshold is expressed as $F_{crit} = F_{crit}(\beta, r)$.

- The energy balance analysis in the shock reveals that, assuming uniform flux factors (energy and momentum), in the back and in the front of the shock, finite-amplitude shocks without (mechanical) energy dissipation are allowed within a single band of wavelength. The limiting conditions are highly sensitive to r , the ratio of the normal stress in the horizontal direction to the normal stress in the vertical direction. The physical consideration of a non-positive (mechanical) energy balance in the shock requires that a second inequality ($b < b'_{crit}$) be satisfied. This inequality, expressed in a similar fashion by Ng and Mei [21] for mud flows, leads to the evaluation of a second threshold expressed as $F'_{crit} = F'_{crit}(\alpha, \beta, r)$.
- A limiting Froude number guarantees for the existence without further conditions of permanent periodic roll waves.
- Integration of the energy dissipation in the stream reveals that the energy budget is a negative function, also in condition of no dissipation in the shock, i.e., the system with permanent waves dissipates more energy than the energy gained from gravity, with a minimum for the MLRW.

Acknowledgements

The author acknowledges support for this work from FIL 2008 and FIL 2009 of the University of Parma. Some computations performed by Sara Daolio during her master thesis are gratefully acknowledged. This paper was revised during his sabbatic leave in CEAMA, Grupo de Dinámica de Flujos Ambientales, University of Granada, Spain, where he was kindly hosted by Miguel A. Losada.

Appendix A

We demonstrate that no solution with an inflection point is possible. In order to have a point of inflection, we should have $\xi_{,Y} = 0$ and $\xi_{,YY} = 0$. Considering the reciprocal of Eq. (7):

$$\xi_{,Y} = \frac{[c^2(\beta - 1) + rgY \cos \theta - \beta K^2/Y^2]}{[gY^5 \sin \theta - a(cY - K)^2]/Y^4} \quad (\text{A.1})$$

the first condition ($\xi_{,Y} = 0$) requires that

$$c^2Y^2(\beta - 1) + rgY^3 \cos \theta - \beta K^2 = 0 \quad (\text{A.2})$$

with the further assumption that

$$gY^5 \sin \theta - a(cY - K)^2 \neq 0. \quad (\text{A.3})$$

The second condition ($\xi_{,YY} = 0$) is imposed by differentiating Eq. (A.1):

$$\begin{aligned} \xi_{,YY} = & \frac{[rg \cos \theta + 2\beta K^2/Y^3]}{\frac{1}{Y^4} [gY^5 \sin \theta - a(cY - K)^2]} \\ & - \frac{[c^2(\beta - 1) + rgY \cos \theta - \beta K^2/Y^2]}{\frac{1}{Y^8} [gY^5 \sin \theta - a(cY - K)^2]^2} \\ & \times \left[g \sin \theta - a(6cK/Y^4 - 2c^2/Y^3 - 4K^2/Y^5) \right] = 0 \quad (\text{A.4}) \end{aligned}$$

which reduces to

$$\xi_{,YY} = \frac{[rg \cos \theta + 2\beta K^2/Y^3]}{\frac{1}{Y^4} [gY^5 \sin \theta - a(cY - K)^2]} = 0 \quad (\text{A.5})$$

due to (A.2). The denominator is different from zero by assumption (Eq. (A.3)), but also because the numerator cannot be zero, since $rg \cos \theta + 2\beta K^2/Y^3$ is always positive.

Appendix B

Defining the four roots as Y_1^* , Y_2^* , Y_3^* , and Y_4^* , with the first two real and with $0 < Y_1^* < Y_2^*$, Eq. (13) can be written as

$$Y_{\xi^*}^* = \sin \theta \frac{(Y^* - Y_1^*)(Y^* - Y_2^*)(Y^* - Y_3^*)(Y^* - Y_4^*)}{Y^{*2}[(\beta - 1)(Y^* + Y_c^*) + r \cos \theta (Y^{*2} + Y_c^* Y^* + Y_c^{*2})]}. \quad (\text{B.1})$$

In addition, for $b < b_{\text{crit}}$ the result also is $0 < Y_1^* < Y_2^* < Y_c^*$. The inverse function representing the wave profile Y^{*-1} can be obtained by integration:

$$\begin{aligned} \xi^* = C + \frac{rY^*}{\tan \theta} + \frac{1}{\sin \theta} f_1 \tan^{-1} \left(\frac{Y^* - \text{Re}(Y_3^*)}{\text{Im}(Y_3^*)} \right) \\ + \frac{1}{\sin \theta} f_2 \ln(Y^* - Y_1^*) + \frac{1}{\sin \theta} f_3 \ln(Y^* - Y_2^*) + \frac{1}{\sin \theta} f_4 \\ \times \ln \left(Y^{*2} - 2Y^* \text{Re}(Y_3^*) + \text{Re}(Y_3^*)^2 + \text{Im}(Y_3^*)^2 \right) \end{aligned} \quad (\text{B.2})$$

where f_1, f_2, f_3 , and f_4 are functions of $Y_1^*, Y_2^*, \text{Re}(Y_3^*), \text{Im}(Y_3^*), Y_c^*, \beta, \theta, r$. $\text{Re}(\dots)$ and $\text{Im}(\dots)$ stand for real and imaginary parts, and Y_3^* is one of the complex roots. The constant can be chosen, making $Y^*(0) = Y_c^*$, and the next waves are obtained by translating the above function of a value equal to a multiple of the length of the wave. The profile has the following equation:

$$\begin{aligned} \xi^*(Y^*) = \frac{r(Y^* - Y_c^*)}{\tan \theta} + \frac{1}{\sin \theta} f_1 \left[\tan^{-1} \left(\frac{Y^* - \text{Re}(Y_3^*)}{\text{Im}(Y_3^*)} \right) \right. \\ \left. - \tan^{-1} \left(\frac{Y_c^* - \text{Re}(Y_3^*)}{\text{Im}(Y_3^*)} \right) \right] + \frac{1}{\sin \theta} f_2 \ln \left(\frac{Y^* - Y_1^*}{Y_c^* - Y_1^*} \right) \\ + \frac{1}{\sin \theta} f_3 \ln \left(\frac{Y^* - Y_2^*}{Y_c^* - Y_2^*} \right) + \frac{1}{\sin \theta} f_4 \\ \times \ln \left(\frac{Y^{*2} - 2Y^* \text{Re}(Y_3^*) + \text{Re}(Y_3^*)^2 + \text{Im}(Y_3^*)^2}{Y_c^{*2} - 2Y_c^* \text{Re}(Y_3^*) + \text{Re}(Y_3^*)^2 + \text{Im}(Y_3^*)^2} \right). \end{aligned} \quad (\text{B.3})$$

Appendix C

Following Ng and Mei [21], we give a definition of critical section and demonstrate that the critical depth is a zero of both numerator and denominator of Eq. (8).

The two conservation laws (1)(a) and (1)(b) can be written in matrix form as

$$\frac{\partial}{\partial t} \begin{Bmatrix} y \\ u \end{Bmatrix} + \mathbf{A} \frac{\partial}{\partial x} \begin{Bmatrix} y \\ u \end{Bmatrix} = \mathbf{B} \quad (\text{C.1})$$

where

$$\mathbf{A} = \begin{bmatrix} u & y \\ (\beta - 1) \frac{u^2}{y} + rg \cos \theta & (2\beta - 1)u \end{bmatrix}, \quad (\text{C.2})$$

$$\mathbf{B} = \begin{Bmatrix} 0 \\ g \sin \theta - \frac{\tau_b}{\rho y} \end{Bmatrix}.$$

\mathbf{A} has the two real distinct eigenvalues $\lambda^\pm = \beta u \pm \sqrt{\beta(\beta - 1)u^2 + rgy \cos \theta}$ corresponding to two families of characteristics:

$$(dx/dt)^\pm = \beta u \pm \sqrt{\beta(\beta - 1)u^2 + rgy \cos \theta}. \quad (\text{C.3})$$

The adjacent characteristics of the positive family $(dx/dt)^+$ can intersect generating a shock. Considering the relation:

$$u = c - \frac{K}{y} \quad (\text{C.4})$$

if y increases u increases and also the inclination of $(dx/dt)^+$ increases. The behaviour is opposite for decreasing y . If part of the wavelength has a decreasing profile, two regions with increasing and decreasing characteristics are present, and a shock could be formed, contradicting the hypothesis of smoothness. As a consequence, the profile has to be monotonically increasing between y_f and y_b and with $(dx/dt)_f^+ < c < (dx/dt)_b^+$.

A critical characteristic must exist in a critical section, where $(dx/dt)_c^+ = c$ with a flow depth $y_f < y_c < y_b$ and a fluid velocity $u_f < u_c < u_b$.

On the left side of $(dx/dt)_c^+ = c$ (where $y_f < y < y_c$ and $u_f < u < u_c$) we have $(dx/dt)^+ < c$. On the right side of $(dx/dt)_c^+ = c$ (where $y_c < y < y_b$ and $u_c < u < u_b$) we have $(dx/dt)^+ > c$.

It can be demonstrated that the characteristics of the negative family, $(dx/dt)^-$ are advancing slowly than c . As a consequence, a disturbance applied on the left side of the critical section will propagate only downstream, whereas a disturbance applied on the right side of the critical section will propagate upstream and downstream. This is the definition of supercritical and sub-critical flows.

Now we demonstrate that the critical depth is a zero of the denominator and of the numerator of the flow profile (Eq. (8)).

The flow in the critical section satisfies the condition:

$$\begin{aligned} c = \beta u_c + \sqrt{\beta(\beta - 1)u_c^2 + rgy_c \cos \theta} \\ \rightarrow c = \beta U_c + \sqrt{\beta(\beta - 1)U_c^2 + rgY_c \cos \theta} \end{aligned} \quad (\text{C.5})$$

which in non-dimensional form, is equivalent to Eq. (9)(a), i.e. Y_c is a zero of the denominator.

We can also demonstrate that the critical depth is also a zero of the numerator.

The left eigenvector \mathbf{L}^+ corresponding to λ^+ has the following two components:

$$L_1^+ = \frac{(\beta - 1)u^2}{y} + rg \cos \theta, \quad (\text{C.6})$$

$$L_2^+ = (\beta - 1)u + \sqrt{\beta(\beta - 1)u^2 + rgy \cos \theta}$$

(by definition, the left eigenvector satisfies the equation $\{L_1^+, L_2^+\} \mathbf{A} = \lambda^+ \{L_1^+, L_2^+\}$).

Multiplying \mathbf{L}^+ by system (C.1) the following equation is obtained:

$$L_1^+ \frac{dy}{dt} + L_2^+ \frac{du}{dt} = L_2^+ \left(g \sin \theta - \frac{\tau_b}{\rho y} \right). \quad (\text{C.7})$$

Along the critical characteristic $(dx/dt)_c^+ = c$ the flow depth y_c and the flow velocity u_c (Y_c and U_c) are invariant:

$$\frac{dy}{dt} = \frac{du}{dt} = 0, \quad \text{if } \frac{dx}{dt} = c. \quad (\text{C.8})$$

As a consequence, the right-hand side of Eq. (C.7) is zero:

$$\begin{aligned} L_2^+ \left(g \sin \theta - \frac{\tau_b}{\rho y} \right) \Big|_{(y_c, u_c)} = 0 \\ \rightarrow L_2^+ \left(g \sin \theta - \frac{\tau_b}{\rho Y} \right) \Big|_{(Y_c, U_c)} = 0. \end{aligned} \quad (\text{C.9})$$

L_2^+ is always positive and the equation reduces to

$$\left(g \sin \theta - \frac{\tau_b}{\rho Y} \right) \Big|_{(Y_c, U_c)} = 0 \quad (\text{C.10})$$

which, in non-dimensional form, is equivalent to Eq. (9)(b), i.e. Y_c is a zero of the numerator.

References

- [1] V. Cornish, *Ocean Waves and Kindred Geophysical Phenomena*, Cambridge University Press, 1934.
- [2] M.K. Smith, The mechanism for the long-wave instability in the liquid films, *J. Fluid Mech.* 217 (1990) 469–485.
- [3] S. Longo, Effects of gradient pressure on resistance law in roll waves, in: Greco, Carravetta, Della Morte (Eds.), *Proceedings of River Flow 2004*, vol. 2, A.A. Balkema Publishers, London, 2004, pp. 885–894.
- [4] R.F. Dressler, Mathematical solution of the problem of roll waves in inclined open channels, *Comm. Pure Appl. Math.* 2 (1949) 149–194.
- [5] T.B. Benjamin, Wave formation in laminar flow down an inclined plane, *J. Fluid Mech.* 2 (1957) 554–574.
- [6] T.B. Benjamin, Corrections to: wave formation in laminar flow down an inclined plane, *J. Fluid Mech.* 3 (1957) 657.
- [7] C.S. Yih, Stability of liquid flow down an inclined plane, *Phys. Fluids* 6 (1963) 321–334.
- [8] C.L. Chen, Unique laminar-flow stability limit based on shallow-water theory, *J. Hydraul. Eng.* 119 (7) (1992) 816–829.
- [9] H.J. Jeffreys, The flow of water in an inclined channel of rectangular section, *Phil. Mag. Ser. (6)* 49 (1925) 793–807.
- [10] J.J. Stoker, *Water Waves*, Wiley Interscience, 1957.
- [11] J.A. Liggett, *Unsteady Flow in Open Channels*, WRP, 1975.
- [12] Y. Iwasa, The criterion for instability of steady uniform flows in open channels, *Mem. Fac. Eng. Kyoto Univ. Japan* 16 (6) (1954) 264–275.
- [13] H.J. Koloseus, J. Davidian, Free surface instabilities correlations, *Geol. Surv. Water-Supply Pap.* 1592-C (1966) 1–72.
- [14] J.E. Berlamont, N. Vanderstappen, Unstable turbulent flow in open channels, *J. Hydraul. Div.* 107 (HY4) (1981) 427–449.
- [15] H. Rouse, Critical analysis of open-channel resistance, *J. Hydraul. Eng.* 91 (HY4) (1965) 1–25.
- [16] M. Rosso, M. Schiara, J. Berlamont, Flow stability and friction factor in rough channels, *J. Hydraul. Eng.* 116 (9) (1990) 1109–1118.
- [17] R.R. Brock, Discussion of critical analysis of open-channel resistance, by H. Rouse, *J. Hydraul. Div.* 92 (HY2) (1966) 403–409.
- [18] R.R. Brock, Development of roll waves in open channels, *W.M. Keck Laboratory of Hydraulics and Water Resources, California Institute of Technology, Report No. KH-R-16*, 1967.
- [19] R.R. Brock, Development of roll wave trains in open channels, *J. Hydraul. Div.* 95 (HY4) (1969) 1401–1427.
- [20] T. Ishihara, Y. Iwagaki, Y. Iwasa, Theory of the roll wave train in laminar water flow on a steep slope surface, *Trans. JSCE* 19 (1954) 46–57 (in Japanese).
- [21] C. Ng, C.C. Mei, Roll waves on a shallow layer of mud modelled as a power-law fluid, *J. Fluid Mech.* 263 (1994) 151–183.
- [22] S.N. Prasad, D. Pal, M.J.M. Römkens, Wave formation on a shallow layer of flowing grains, *J. Fluid Mech.* 413 (2000) 89–110.
- [23] P.G. Mayer, Roll waves and slug flows in inclined open channels, *J. Hydraul. Div.* 85 (HY7) (1959) 99–141.
- [24] P.Y. Julien, D.M. Hartley, Formation of roll waves in laminar sheet flow, Rep. CER84-85PYJ-DMH18, Department of Civil Engineering, Colorado State University, 1985.
- [25] P.Y. Julien, D.M. Hartley, Formation of roll waves in laminar sheet flow, *J. Hydraul. Res.* 24 (1986) 5–17.
- [26] V.M. Ponce, M.B. Maisner, Verification of theory of roll wave formation, *J. Hydraul. Eng.* 119 (6) (1993) 768–773.
- [27] P.L. Kapitza, Wave flow of thin layers of a viscous fluid, *Zh. Eksp. Teor. Fiz.* 18 (1948) 3–28 (Also in *Collected Papers of P.L. Kapitza*, vol. II, 1938–1964, Pergamon Press, 662–709, 1965).
- [28] C. Kranenburg, On the evolution of roll waves, *J. Fluid Mech.* 245 (1992) 249–261.
- [29] C. Montuori, La formazione spontanea dei treni d'onde su canali a pendenza molto forte, *L'Energ. Elettr.* 38 (2) (1961) 127–141 (in Italian); Also available, in: *Spontaneous formation of wave trains in channels with a very steep slope*, WES Translation 65-12 US Army Engineer Waterway Experiment Station, Vicksburg, MI, 1965.
- [30] R.A. Bagnold, Experiments on a gravity-free dispersion of large solid spheres in a Newtonian fluid under shear, *Proc. R. Soc. Lond. Ser. A* 225 (1954) 49–63.
- [31] C.L. Chen, C.H. Ling, Granular-flow rheology: role of shear-rate number in transition regime, *J. Eng. Mech.* 122 (5) (1996) 469–480.
- [32] C.L. Chen, C.H. Ling, Rheological equations in asymptotic regimes of granular flow, *J. Eng. Mech.* 124 (3) (1998) 301–310.
- [33] M.L. Hunt, R. Zenit, C.S. Campbell, C.E. Brennen, Revisiting the 1954 suspension experiments of R.A. Bagnold, *J. Fluid Mech.* 452 (2002) 1–24.
- [34] T. Takahashi, *Debris Flow*, in: *IAHR Monograph Series*, Balkema, Rotterdam, 1991.
- [35] S. Okubo, H. Ikeya, Y. Ishikawa, T. Yamada, Development of new methods for countermeasures against debris flows, in: Armanini, Michiue (Eds.), *Recent Developments on Debris Flows*, in: *Lecture Notes in Earth Sciences*, vol. 64, Springer-Verlag, 1997.
- [36] J.M.N.T. Gray, J.M. Wieland, K. Hutter, Gravity-driven free surface flow of granular avalanches over complex basal topography, *Proc. R. Soc. Lond. Ser. A* 455 (1999) 573–600.
- [37] D. Ertas, G.S. Grest, T.H. Halsey, D. Levine, E. Silbert, Gravity driven dense granular flows, *Europhys. Lett.* 56 (2001) 214–220.
- [38] V.T. Chow, *Open Channel Hydraulics*, McGraw Hill, 1959.
- [39] G.B. Whitham, *Linear and Nonlinear Waves*, Wiley-Interscience Publication, John Wiley and Sons, New York, 1974.
- [40] C. Hwang, J. Chen, J. Wang, J. Lin, Linear stability of power-law liquid film flows down an inclined plane, *J. Phys. D: Appl. Phys.* 27 (1994) 2297–2301.